Dynamics of glasses

2001 J. Phys.: Condens. Matter 13 7827

(http://iopscience.iop.org/0953-8984/13/34/322)

INSTITUTE OF PHYSICS PUBLISHING JOURNAL OF PHYSICS: CONDENSED MATTER

J. Phys.: Condens. Matter **13** (2001) 7827–7846 PII: S0953-8984(01)25623-9

Dynamics of glasses

U Buchenau

Institut für Festkörperforschung, Forschungszentrum Jülich, Postfach 1913, 52425 Jülich, Germany

Received 8 June 2001, in final form 8 June 2001
Published 9 August 2001
Online at stacks.iop.org/JPhysCM/13/7827

E-mail: u.buchenau@fz-juelich.de

Abstract

The dynamics of glasses is characterized by disorder-specific, more or less localized modes: tunnelling states, soft vibrations and classical relaxation. These modes coexist and interact with the sound waves, giving rise to anomalies in the thermal properties of glasses at low temperatures. At higher temperatures, the low-frequency dynamics is dominated by the classical secondary relaxation, which crosses over to the primary relaxation at the glass transition.

The present article describes first the low-temperature glass anomalies in the heat capacity and in the thermal conductivity. Then, three closely related models are reviewed: the tunnelling model, the soft-potential model and the Gilroy–Phillips model. The latter allows a joint quantitative description of primary and secondary relaxation, giving a new view on the glass transition. Finally, recent inelastic x-ray, light and neutron scattering experiments on the mixture of sound waves and other modes in glasses are discussed.

1. Introduction

Following Jäckle (1987), one defines a glass as an amorphous solid obtained by cooling a liquid through the glass transition, retaining the disordered liquid structure.

From the point of view of elasticity theory, a glass is a very simple solid, elastically isotropic, described by a density ρ, a bulk modulus B and a shear modulus G. Consequently, one has isotropic longitudinal and transverse sound velocities, respectively. The complications begin when one looks for the absorption of these sound waves as a function of frequency and temperature. Then one realizes that there is a multitude of other excitations coexisting and interacting with the sound waves.

The key to the understanding of this multitude lies in the multiminimum concept of the glass: though the disordered structure no longer flows, there are still many minima of the potential energy. One has to reckon with low and high barriers between them, and one has to take into account the energy difference between neighbouring minima of the glass. This was first done in the tunnelling model for the glass anomalies below 1 K (Phillips 1972,

Anderson *et al* 1972). The concept was applied to the classical relaxation in the glass phase, called secondary relaxation to distinguish it from the primary relaxation at the glass transition, by Gilroy and Phillips (1981). In the same decade, the tunnelling model was extended to treat the crossover from tunnelling to low-frequency localized vibration on one side, and to classical relaxation on the other in terms of the soft-potential model (Karpov *et al* 1983, Ilin *et al* 1987).

The present paper begins in section 2 with a short description of the universal low-temperature anomalies of glasses (Phillips 1981). Section 3 continues with their modelling, the tunnelling model and its two extensions, the soft-potential model for the crossover from tunnelling to vibration and the Gilroy–Phillips model for the classical secondary relaxation of the glass phase. It has recently been shown (Buchenau 2000) that the Gilroy–Phillips formalism can be again extended to describe the primary relaxation at the glass transition, giving a new and surprising view of the old glass transition puzzles. This joint description of flow process and secondary relaxation in the glass phase will be presented in section 4.

Section 5 reviews x-ray, light and neutron experiments to investigate sound waves and other modes in glasses, giving a feeling for the possibilities and limitations of the different scattering techniques at the present stage. Section 6 gives a summary and the conclusions.

2. Low-temperature anomalies of glasses

Whatever problems we may have to understand the dynamics of glasses, there is one part which is well understood, namely the sound waves at low frequencies. For these, the glass is simply an isotropic elastic medium, described by its density ρ and its two sound velocities v_l and v_t for longitudinal and transverse sound waves, respectively. In terms of the elastic constants c_{11} and c_{44}, one has

$$\rho v_l^2 = c_{11} \qquad \rho v_t^2 = c_{44}. \tag{1}$$

The elastic constants can in turn be expressed by the bulk modulus B and the shear modulus G

$$c_{11} = B + \frac{4G}{3} \qquad c_{44} = G. \tag{2}$$

Debye's famous consideration yields a density $V_g/(2\pi)^3$ in wavevector space for these sound waves, where V_g is the volume of the glass. For a given wavevector direction, one has one longitudinal branch, vibrating parallel to the wavevector, and two transverse branches with the vibrational amplitude perpendicular to the wavevector.

The total density of sound waves (normalized to 1) is

$$g(\omega) = \frac{3\omega^2}{\omega_D^3} \tag{3}$$

with the Debye frequency ω_D given by

$$\omega_D^3 = \frac{18\pi^2\rho}{\overline{M}(1/v_l^3 + 2/v_t^3)}. \tag{4}$$

Here $\overline{M}$ is the average atomic mass.

There is general agreement that the Debye model is a valid description of the sound waves in glasses at low frequencies, at least up to about 300 GHz. What happens above that frequency is again controversial. Neutron and x-ray experiments are able to supply information at these higher frequencies. We will return to this point in section 5.

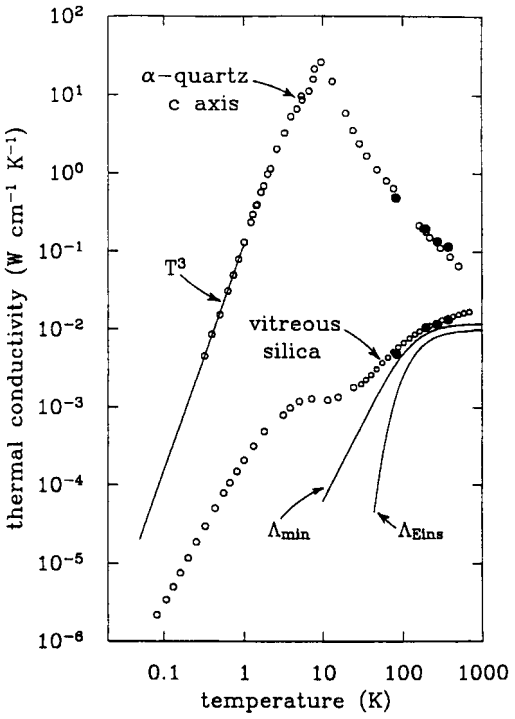

Figure 1. Thermal conductivity of crystalline and amorphous SiO_2, taken from Cahill D 1989 *Thesis* Cornell.

In any case, the contribution of the sound waves to the low-temperature heat capacity of a glass with volume V_g will be well described by

$$c_V = k_B \frac{4\pi}{3} V_g \left(\frac{1}{v_l^3} + \frac{2}{v_t^3} \right) T^3 \tag{5}$$

and the thermal conductivity κ of these sound waves should follow the textbook relation

$$\kappa = \frac{1}{3V_g} c_V \overline{v} l \tag{6}$$

where $\overline{v}$ is the average sound velocity and l is the mean free path of the sound waves in the glass. Thus one would expect a T^3 behaviour of both quantities at low temperatures.

Experimental reality is completely different (Zeller and Pohl 1971). Figure 1 shows a measurement of the thermal conductivity on a log–log scale against the temperature T, comparing crystalline quartz with vitreous silica. One sees the Debye expectation fulfilled in crystalline quartz; taking the absolute values, one finds a mean free path of the order of the sample dimensions, showing that the main phonon scattering mechanism in the crystal is boundary scattering. But the glass rather shows an approximate T^2-law, orders of magnitude below the crystal values, which then even bends over into a plateau at 5 K. Obviously, there is a very strong scattering mechanism for the phonons in the glass, which is absent in the crystal.

One gets a hint at the reason for this scattering by looking at the heat capacity, which shows many additional excitations on top of the sound waves. Figure 2 shows the specific heat C_p per g, plotted as C_p/T^3, again in a log–log scale against T. In this plot, the sound wave contribution of equation (5) is a constant at 0.8 μJ g^{-1} K^4, as one easily calculates from the density and the sound velocities. The measured value at 0.2 K is a factor of 40 higher. The temperature dependence of C_p between 0.2 and 1 K is more or less linear, $T^{1.2}$, indicating a

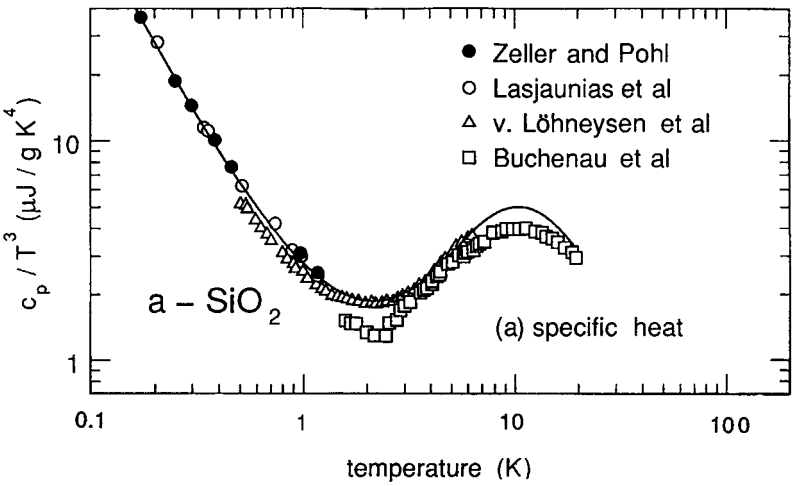

Figure 2. Specific heat of amorphous SiO_2, plotted as C_p/T^3 against T in a log–log scale.

more or less constant density of states. Above 1 K, the behaviour changes, indicating a stronger and stronger increase of the number of additional modes with increasing level splitting. One sees level splittings of about 0.4 meV, corresponding to frequencies of 100 GHz, in the specific heat at 1 K. Obviously, something happens to the modes around this frequency. The onset of the plateau of the thermal conductivity occurs at about the same temperature, suggesting that the two things have something to do with each other. The increase in the number of additional modes leads to an increase in the phonon scattering.

3. Modelling dynamics in disorder

3.1. The tunnelling model

The glass anomalies below 1 K can be explained in terms of the phenomenological tunnelling model (Phillips 1972, Anderson *et al* 1972), assuming tunnelling in asymmetric double-well potentials (figure 3). The essential point of the model is to consider the barrier height V and the asymmetry Δ as *independent* variables, both of which are evenly distributed. Under this assumption, one can calculate the resulting distribution of tunnelling states. In order to derive their contribution to the specific heat and to the thermal conductivity, one needs their coupling to the sound waves. This is described by two coupling constants γ_l and γ_t, defined for the uniaxial strain $\epsilon_l = \epsilon_{11}$ of the longitudinal sound wave and for the shear strain $\epsilon_t = \epsilon_{11} - \epsilon_{22}$ of the transverse sound wave, respectively. The coupling is such that the asymmetry changes from Δ in the unstrained glass to $\Delta + \gamma\epsilon$ in the strained glass.

With this coupling and the given Debye density of sound waves, one can determine the relaxation time of a given tunnelling state to calculate its contribution to the specific heat, the thermal conductivity and the ultrasonic absorption. One gets two contributions to the ultrasonic absorption, resonant and relaxational ones. Since one deals with a two-level state, the resonant interaction should saturate with increasing ultrasonic power, when the two levels get equally populated. This was indeed found in experiment (Hunklinger *et al* 1972), giving strong support to the tunnelling idea. More details on the model and on its comparison to experiment can be found in Phillips' book (Phillips 1981). Though not every experiment is

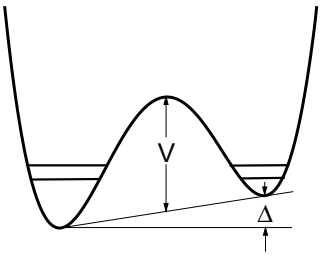

Figure 3. Tunnelling levels in an asymmetric double-well potential (schematic).

well reproduced, on the whole the model turned out to be able to describe the bulk of the glassy anomalies below 1 K in many glasses with three parameters, the two coupling constants and an average density $\overline{P}$.

The tunnelling model does not explain the plateau in the thermal conductivity and the rise to the peak in C_p/T^3. This peak corresponds also to a peak in Raman and neutron spectra, the boson peak (see section 5). In the scattering experiments, one can look at the temperature dependence of the inelastic scattering at the boson peak frequency. One finds the linear increase with temperature expected for harmonic vibrations (for a tunnelling state, the intensity would disappear as soon as the two levels are equally populated). This shows that the plateau and the rise to the peak must be explained in terms of a crossover from tunnelling states to low-frequency vibrations, which resonantly scatter the sound waves. In order to describe this crossover, the tunnelling model was extended to the soft-potential model described in the next subsection.

3.2. The soft-potential model

If one wants to describe double-well and single-well potentials with the same potential form, one is forced to include a stabilizing fourth-order term in the expansion. Otherwise one never gets the negative curvature of the double-well potential at the top of the barrier, together with a rise of the potential at the sides.

If one further wants a continuous distribution of asymmetries and barrier heights, the proper form to choose is

$$E_{pot}(x) = W(D_1 x + D_2 x^2 + x^4) \tag{7}$$

where the multitude of different modes results from a broad distribution of D_1 and D_2 around the value zero. W is an energy and x is a dimensionless measure of the mode displacement. The most reasonable definition, which has been followed throughout in the literature (Karpov *et al* 1983, Ilin *et al* 1987), is to take W as the zero-point energy in the purely quartic potential $D_1 = D_2 = 0$, which requires a kinetic mode energy of the form

$$E_{kin} = \frac{\hbar^2}{4W}\dot{x}^2. \tag{8}$$

With this choice, W is the crossover energy between vibrations and tunnelling states: there can be no greater tunnelling splitting than W (at least not for symmetric potentials), and there can be no lower vibrational frequency than $W/\hbar$.

As for the tunnelling states, one very nearly (not exactly) reproduces the tunnelling model postulating a constant distribution P_s both in D_1 and D_2, because one gets a practically continuous distribution of barrier heights and asymmetries.

The coupling between sound waves and local modes is now given by a bilinear term in the strain and the mode coordinate

$$\delta V_l = \Lambda_l x \epsilon_l \qquad \delta V_t = \Lambda_t x \epsilon_t. \tag{9}$$

The coupling is conveniently expressed in terms of two dimensionless parameter combinations of order 10^{-4}

$$C_l = \frac{P_s \Lambda_l^2}{W \rho v_l^2} \qquad C_t = \frac{P_s \Lambda_t^2}{W \rho v_t^2}. \tag{10}$$

C_l and C_t are defined in such a way that they are very nearly equal to (about a factor of 0.9 smaller than) the corresponding parameter combinations of the tunnelling model, which are denoted by the same letters.

With these definitions and the four parameters W, P_s, C_l and C_t one can describe not only the tunnelling states below 1 K, but also the plateau in the thermal conductivity in figure 1 and the minimum in C_p/T^3 in figure 2. In addition, one can describe the crossover in the ultrasonic attenuation from the tunnelling plateau to thermally activated classical relaxation with the same parameters (Ramos and Buchenau 1997).

However, the description breaks down as one goes to still higher frequencies or temperatures. The assumption of a P_s which is constant everywhere fails to describe the boson peak; if it were true, one should find a rise in the spectrum $\sim\omega^2$ without end. At the relaxational side, one should find a rise of the internal friction $\sim T^{3/4}$, again without end. Neither of the two is observed in experiment (Ramos and Buchenau 1997). Thus one has to look for a more flexible extension of the tunnelling model to explain the dynamics of glasses at higher temperature. On the relaxational side, such a flexible extension exists: the Gilroy–Phillips model (Gilroy and Phillips 1981), which can not only be used to describe the secondary relaxation in the glass phase, but even the primary relaxation of the flow process at the glass transition and above.

3.3. The Gilroy–Phillips model

3.3.1. Arrhenius and Vogel–Fulcher laws. Classical relaxation in glasses, sometimes also called secondary relaxation to distinguish it from the primary relaxation at the glass transition, is generally believed to be well described in terms of the Arrhenius–Kramers picture (Kramers 1940), with a relaxation time τ_V given by the Arrhenius relation

$$\tau_V = \tau_0 \, \mathrm{e}^{V/k_B T} \tag{11}$$

where τ_0 is a microscopic time of the order of 10^{-13} s, V is the energy of the barrier between two energy minima of the system and T is the temperature.

In contrast, the primary relaxation or α-process, the onset of the flow process at the glass transition temperature T_g and above, seems to follow a much steeper law (Böhmer *et al* 1993, Ediger *et al* 1996)

$$\tau_\alpha = \tau_0 \, \mathrm{e}^{A/(T-T_0)} \tag{12}$$

where A and T_0 are constants with the dimension of a temperature. This is the well known empirical Vogel–Fulcher–Tamman (VFT) or Williams–Landel–Ferry (WLF) equation. T_0, the Vogel–Fulcher temperature, is smaller than T_g; the closer it lies to T_g, the more fragile is the glass former.

Since the Arrhenius law has a sound microscopic background (Kramers 1940) and the VFT or WLF equation has not, it seems reasonable to build a joint quantitative description on the former, bearing in mind the physical difference of the two processes (Buchenau 2000). The proper basis for such an attempt is the Gilroy–Phillips model (Gilroy and Phillips 1981) described in this subsection.

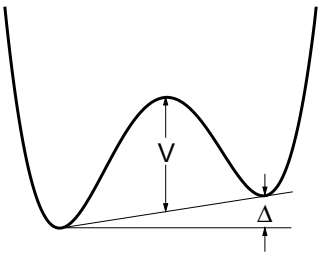

Figure 4. Asymmetric double-well potential with barrier height V and asymmetry Δ as a function of a generalized coordinate.

3.3.2. The asymmetric double-well potential. Let us denote the shear strain by ϵ, the shear stress by σ and the (infinite-frequency) shear modulus by G. G will generally depend on the temperature T.

The structural relaxation is taken to be a superposition of independent Debye relaxation centres in asymmetric double-well potentials with two minima, as shown in figure 4. The energy of the left minimum is $-\Delta/2$ and the energy of the right minimum is $+\Delta/2$. The height of the barrier is V.

As in the tunnelling model, the interaction between the shear strain and the Debye relaxation centre is described by the change of the asymmetry Δ under the influence of the strain. The interaction is characterized by the coupling parameter γ, leading to an asymmetry $\Delta + \gamma\epsilon$ of the relaxation in the strained glass. γ must be considered to depend both on V and Δ.

The free energy F of the relaxation centre reads

$$F = -k_B T \ln\left[2\cosh\left(\frac{\Delta + \gamma\epsilon}{2k_B T}\right)\right] \tag{13}$$

which has the second derivative with respect to the shear distortion ϵ

$$\frac{\partial^2 F}{\partial \epsilon^2} = -\frac{\gamma^2}{4k_B T \cosh^2(\Delta/2k_B T)}. \tag{14}$$

The second derivative determines the contribution of that specific relaxing entity to the difference between the shear moduli at infinite and zero frequency. The equation shows that the main influence on the shear modulus is due to relaxation in potentials with asymmetries smaller than $k_B T$; for larger asymmetries the influence decreases rapidly because of the square of the hyperbolic cosine in the denominator.

3.3.3. The barrier density function $f(V)$. We want to calculate the frequency dependence of the shear modulus under the assumption of slowly varying distribution functions in the parameters V and Δ. In detail, we assume a number density of relaxing entities $n(V, \Delta)$ and an average coupling constant $\gamma(V, \Delta)$ which are both approximately constant if either V or Δ is varied by an amount of the order of the thermal energy $k_B T$.

Under this assumption, it is safe to neglect as well the influence of the asymmetry on the relaxation time. We assume the relaxation time τ_V to be given by the Arrhenius equation (11).

We then integrate over the asymmetry Δ to obtain the step δG between the shear moduli at infinite and zero frequency from all relaxation centres with barrier height between V and $V + \mathrm{d}V$

$$\delta G = \mathrm{d}V \int_{-\infty}^{\infty} \frac{\gamma^2 n(V, \Delta)\,\mathrm{d}\Delta}{4k_B T \cosh^2(\Delta/2k_B T)}. \tag{15}$$

Since one has only contributions in the near neighbourhood of $\Delta = 0$, where $n(V, \Delta) \approx n(V, 0)$, and since

$$\int_{-\infty}^{\infty} \frac{\mathrm{d}\Delta}{\cosh^2(\Delta/2k_BT)} = 4k_BT \tag{16}$$

one finds

$$\delta G = \gamma^2 n(V, 0)\,\mathrm{d}V. \tag{17}$$

This is different from a single relaxation in a symmetric potential, where the step in the modulus is inversely proportional to the temperature. The physical reason for this difference is clear: as the temperature rises, relaxation centres with higher and higher asymmetry begin to contribute to the step in the modulus. This is an important difference between relaxation in crystals and relaxation in disordered matter.

The temperature-independent step in the modulus is determined by the barrier density function $f(V)$, defined by

$$f(V) = \frac{\gamma^2 n(V, 0)}{G}. \tag{18}$$

This parameter combination can be argued to remain independent of temperature, even if G varies with temperature, considering the relaxing entity as a small misfit region in an elastic medium (Mura 1982), a misfit region which is able to change the sign of the misfit by jumping over the barrier. Here, however, this argument will not be given in detail.

The frequency dependence of the complex shear modulus at the frequency ω and the temperature T reads

$$\frac{G'(\omega, T)}{G} = \frac{G_e}{G} + \int_0^{\infty} f(V) \frac{\omega^2\tau_V^2\,\mathrm{d}V}{1 + \omega^2\tau_V^2} \tag{19}$$

$$\frac{G''(\omega, T)}{G} = \int_0^{\infty} f(V) \frac{\omega\tau_V\,\mathrm{d}V}{1 + \omega^2\tau_V^2} \tag{20}$$

where τ_V is a function of V by the Arrhenius relation, equation (11), and G_e is the zero-frequency modulus after the decay of all the relaxations in the system.

In a viscoelastic liquid, the zero-frequency modulus $G_e = 0$. In the high-frequency limit, equation (19) implies an important sum rule for the barrier density function

$$\int_0^{\infty} f(V)\,\mathrm{d}V = 1. \tag{21}$$

The two equations (19) and (20) describe the real and the imaginary part of the frequency-dependent shear modulus at all frequencies and temperatures. As long as one can reckon with a temperature-independent number of uncoupled relaxation centres, the barrier density function $f(V)$ remains temperature independent.

But even if $f(V)$ depends on temperature, it can still be formally used to characterize the shear relaxation. The advantage of the choice of $f(V)$ lies in the possibility to distinguish the trivial Arrhenius temperature dependence from other, non-trivial temperature changes. These non-trivial temperature changes will then be reflected in a temperature dependence of $f(V)$. The inclusion of the flow process in such a description (Buchenau 2000) will be treated in the next section.

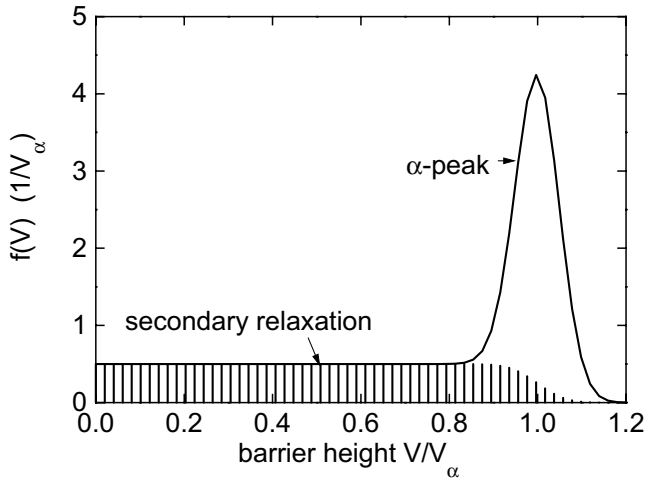

Figure 5. Secondary barrier density function $f_s(V)$ (the shaded area), together with the cutoff by the α-relaxation peak (schematic).

4. Secondary relaxation and glass transition

4.1. Primary and secondary barrier density function

It is quite clear that one needs to distinguish secondary and primary processes, because their physical mechanism is different. To describe both within the Gilroy–Phillips formalism with a barrier density function, one has to distinguish between $f_s(V)$, the secondary barrier density function of the secondary Arrhenius relaxation, and $f_\alpha(V)$, the primary barrier density function for the primary α-process or flow process (see figure 5).

As is well established (Ferry 1980), the shape of the primary relaxation is independent of the temperature; there is just a temperature shift of the characteristic relaxation time τ_α. This is the time–temperature scaling of the α-process, sometimes also denoted as thermorheological simplicity. It implies that the primary barrier density function $f_\alpha(V)$ is an essentially temperature-independent function of $V - V_\alpha(T)$, where $V_\alpha(T)$ denotes the maximum of this strongly peaked function. From the Vogel–Fulcher law, equation (12), one expects a divergence of the fictive Arrhenius barrier $V_\alpha(T)$ towards the Vogel–Fulcher temperature T_0.

If time–temperature scaling holds, the weight w_α of the α-process, given by

$$w_\alpha = \int_0^\infty f_\alpha(V)\,\mathrm{d}V \tag{22}$$

should be temperature-independent. In the comparison to experiment, we will see that w_α tends to be close to a half.

What does this imply for the secondary relaxations? The α-process is also an upper cutoff for the secondary relaxation; at the end of the process, the long-time shear modulus is zero. If a secondary relaxation barrier is too high, the relaxing entity will flow away before it has a chance to jump. Therefore there is a steep cutoff for the secondary barrier density function $f_s(V)$ at $V_\alpha(T)$. According to the sum rule, equation (21),

$$\int_0^{V_\alpha(T)} f_s(V)\,\mathrm{d}V = 1 - w_\alpha = \text{constant} \approx \frac{1}{2}. \tag{23}$$

With this sum rule, the decrease of $V_\alpha(T)$ with increasing temperature implies that the secondary barrier density function $f_s(V)$ *must increase* with increasing temperature. This

increase will be stronger for more fragile glass formers. Such a connection between the fragility and the rise of the fast process above T_g has been indeed postulated empirically (Angell 1995); the Gilroy–Phillips formalism quantifies this connection.

The increase of $f_s(V)$ above the glass temperature can be characterized to first order by

$$f_s(V) = f_s(V, T_g)\left[1 + \alpha_s(V)\frac{T - T_g}{T_g}\right]. \tag{24}$$

4.2. The generic case $f_s(V) =$ constant

The deep implications of the Gilroy–Phillips formulation of the α-process are more clearly seen in the simplest possible case, shown in figure 5. Let us assume $f_s(V) =$ constant and $\alpha_s(V) =$ constant. If the rise of $f_s(V)$ with temperature is strictly linear, the Vogel–Fulcher temperature T_0 is given by

$$T_0 = T_g\left(1 - \frac{1}{\alpha_s}\right). \tag{25}$$

It is obvious how this comes about: at T_0, the density of secondary processes extrapolates to zero. Thus one has to proceed to infinitely high barriers to satisfy the sum rule (23). This gives a completely new view on the puzzling fragility of glass formers: the abnormal temperature dependence is a consequence of the time–temperature scaling of the α-process and of a strictly linear rise of the number of secondary relaxing units with temperature.

The decrease of the secondary barrier density function $f_s(V)$ implies a decrease of the number of minima of the glass former. Thus one gets an equality (Angell and Rao 1972) between the Vogel–Fulcher and the Kauzmann temperature T_K, the latter being defined as the temperature where the excess entropy of the glass former over the corresponding crystalline system extrapolates to zero. If there are no minima between which the glass former can jump, there is no excess entropy, the old Adam–Gibbs idea (Adam and Gibbs 1965).

Note that equation (25) for the Vogel–Fulcher or Kauzmann temperature holds not only in the generic case of a constant secondary barrier density function, but for any $f_s(V)$, as long as one can reckon with the same strictly linear temperature rise of the function for all V.

It should be noted further that this is not a model, but a description. The Gilroy–Phillips formulation does not really explain the puzzling features of the glass transition, the fragility and the entropy crisis. But it supplies a description which allows us to look for a new kind of explanation.

4.3. An example: polystyrene

The amorphous polymer polystyrene is one of the most fragile substances (Böhmer *et al* 1993), where one can rely on a large number of experimental data, both at low temperatures and at the glass transition.

The low-temperature data were evaluated for temperatures above 10 K; at that limiting temperature, one can begin to reckon with the validity of the Kramers picture (Kramers 1940). Figure 6 shows a compilation of many mechanical low-temperature data: torsion pendulum data at 1 Hz (Schwarzl 1990, figure 9.16), at 6 Hz (Sinnott 1962), vibrating reed data at 3, 34 and 87 kHz (Nittke *et al* 1995, Yano and Wada 1971, Topp and Cahill 1996) and Brillouin damping of longitudinal sound waves at 10 GHz (Sokolov *et al* 1997). The data cannot be said to coincide perfectly in this Gilroy–Phillips evaluation; nevertheless, the agreement is good enough to support the concept of a constant number density of uncoupled relaxation centres. There is no systematic variation with frequency; one rather has the impression that

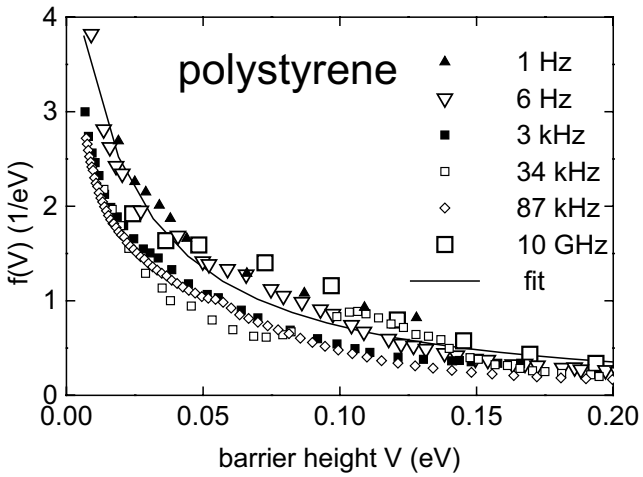

Figure 6. Secondary barrier density function $f_s(V)$ calculated from literature data of the mechanical damping of amorphous polystyrene in the glass phase at different frequencies. For references see the text. The curve is a fit; the same fit is also shown in figures 7, 8 and 9.

the differences stem from the different sample preparation of these seven measurements. The curve in figure 6 represents the fit of $f_s(V)$ to these mechanical data. It is seen that $f_s(V)$ rises towards low barriers, as one would indeed expect from the soft-potential model, which predicts a proportionality to $V^{-1/4}$. But the fit falls below the soft-potential expectation even at rather low barriers, similar to observations in other glasses (Ramos and Buchenau 1997).

Figure 7 compares the same fit to the evaluation of Raman (Surovtsev *et al* 1998) and neutron (Koizumi *et al*) data. The good agreement between data points and the mechanical data fit curve in figure 7 corroborates the earlier conclusion (Surovtsev *et al* 1998) of a temperature-independent $f_s(V)$ in the glass phase of polystyrene. Note that the earlier conclusion does not stem from a comparison of Raman and mechanical data, but rather from a comparison of Raman data at three different temperatures, namely 100, 200 and 300 K. The two different ways to check the temperature behaviour of $f_s(V)$ in the glass phase provide the same result.

This temperature independence, however, no longer holds in the undercooled liquid phase, above the glass temperature of 372 K of polystyrene. Figure 8 shows neutron (Koizumi *et al*) and longitudinal sound wave damping data from the Brillouin technique (Patterson 1977) above T_g. In order to relate to the preceding figures, $f(V)$ is again plotted against the barrier height V. This implies that one sees the onset of the increase of $f_s(V)$ with increasing temperature at different values of V in the two techniques, at 0.074 eV for the neutrons and at 0.163 eV for the Brillouin data. Note that in both cases the frequency is too high to see the α-process at the temperatures of the measurement.

We conclude that $f_s(V)$ does indeed increase above T_g, as postulated above on the basis of the sum rule for $f(V)$, equation (21), and on the basis of the temperature dependence of the α-process. The rise of $f_s(V)$ above T_g can be characterized by the linear relation equation (24) with $\alpha_s = 7.7 \pm 1$ for the neutron data and $\alpha_s = 10 \pm 3$ for the Brillouin data (in the latter case, the large error is due to the small number of points and the insecurity of the value at T_g), within experimental error the same temperature coefficient for both sets of data.

Figure 9 shows $f_s(V)$ for polystyrene over the whole barrier range, together with the results of a torsion pendulum measurement at 1 Hz up to T_g (Schwarzl 1990, figure 9.16), an ultrasonic measurement just below T_g (Sahnoune *et al* 1996) and the neutron result up to T_g (Koizumi

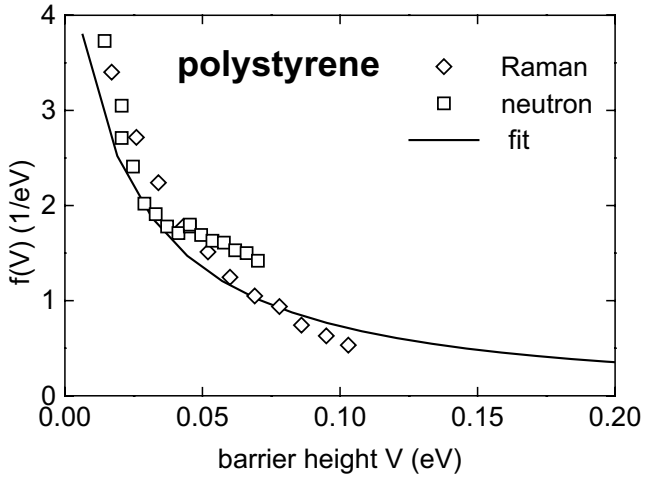

Figure 7. Secondary barrier density function $f_s(V)$ calculated from literature data of neutron and Raman scattering from amorphous polystyrene in the glass phase. For references see the text.

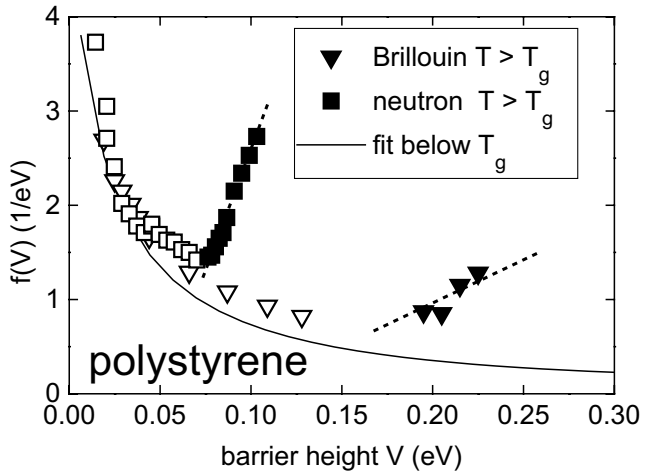

Figure 8. Secondary barrier density function $f_s(V)$ calculated from literature data of neutron and Brillouin data of amorphous polystyrene, both in the glass phase and above the glass temperature T_g. For references see the text.

et al). The shaded area represents $f_s(V)$; the α-peak above 1 eV will be discussed below.

The α-process is characterized by the position $V_\alpha(T)$, the full width at half maximum Δ_α of $f_\alpha(V)$ and the weight w_α. The latter two should be temperature independent. Let us define $V_\alpha(T_g) = 15k_BT_g \ln(10)$ in order to have the corresponding relaxation time at 100 s, and let us choose a Gaussian for the primary barrier density function $f_\alpha(V)$.

If one knows $f_s(V)$ from measurements in the glass phase, w_α can be calculated from the sum rule, equation (23). In the case of polystyrene, one finds $w_\alpha = 0.54$ for the fit function in figure 9.

The width $\Delta_\alpha = 0.107$ eV, the glass temperature $T_g = 372$ K and the coefficient $\alpha_s = 6.9 \pm 0.1$ were fitted to creep data (Plazek and O'Rourke 1971) of polystyrene with a molecular weight of 600 000 g mol^{-1}, data which are also treated in Ferry's book (Ferry

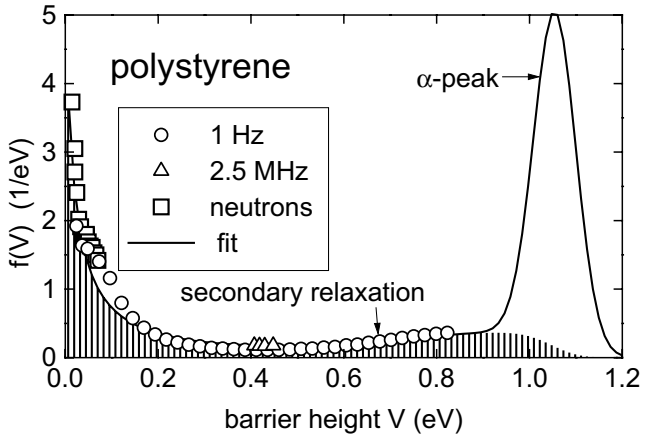

Figure 9. Secondary barrier density function $f_s(V)$ calculated from literature mechanical damping and neutron data of amorphous polystyrene up to the glass transition. The peak at the end shows the Gaussian $f_\alpha(V)$ describing the α-process at the glass temperature T_g. For references see the text.

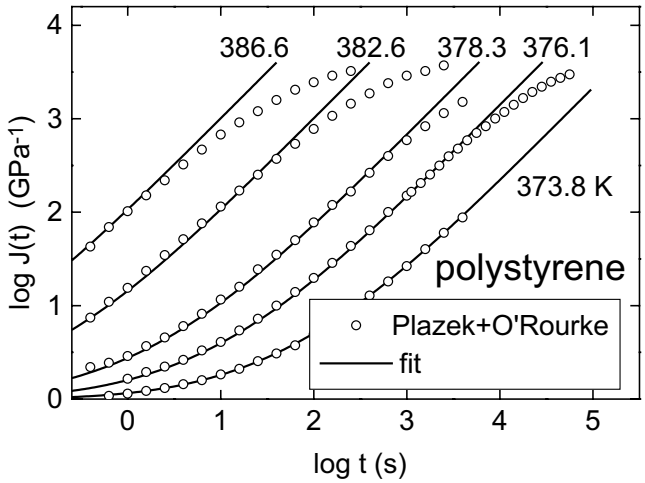

Figure 10. Creep data of the α-process in polystyrene at the glass transition (for reference see the text), together with a fit in terms of $f(V)$.

1980) and which are shown in figure 10. The fit requires as an additional parameter the infinite-frequency modulus $G = 1.69$ GPa at 373.8 K. Together with the low-temperature data and the known density variation of polystyrene with temperature (Schwarzl 1990, figure 6.12), one calculates a Grüneisen $\Gamma_g = 3.8$ for G in polystyrene. With this value, one can also calculate G for higher temperatures.

As seen in figure 10, one can describe the temperature shift of the α-process with an appropriate rise of $f_s(V)$ above T_g. The sum rule, equation (23), forces a temperature shift of $V_\alpha(T)$, which in turn provides the experimentally observed shift factors towards higher temperatures.

The scheme works quite well up to three decades in compliance; for still higher compliances, one gets into the plateau regime from the chain entanglement (Ferry 1980),

which is beyond the present considerations.

The coefficient $\alpha_s = 6.9 \pm 0.1$ for polystyrene, obtained from the temperature dependence of the shift factors in figure 10, agrees within experimental error with the values $\alpha_s = 7.7 \pm 1$ and $\alpha_s = 10 \pm 3$ determined from neutron and Brillouin data above T_g (see figure 8).

The example shows that the Gilroy–Phillips formalism is indeed able to give a reasonable joint description of primary and secondary relaxation, helping to understand the glass transition from the glass side. It does not help, however, to understand the vibrational dynamics of glasses treated in the next section in the context of scattering experiments.

5. Inelastic scattering from glasses

5.1. Scattering from sound waves

The inelastic coherent scattering from sound waves in glasses (Carpenter and Pelizzari 1975) consists of two parts: Brillouin scattering at low momentum transfer Q from the longitudinal sound waves alone and umklapp scattering from both longitudinal and transverse sound waves at higher momentum transfer. In the classical high-temperature approximation, the Brillouin scattering is given by

$$S_{Brill}(Q,\omega) = \frac{k_B T Q^2}{2\overline{M}\omega^2}\delta(\omega \pm v_l Q) \tag{26}$$

with k_B as Boltzmann's constant, $\overline{M}$ as the average atomic mass and v_l as the longitudinal sound velocity. For a damped harmonic oscillator, the two δ-functions have to be replaced by the DHO equation

$$F(\omega) = \frac{2}{\pi}\frac{\Omega^2\Gamma}{(\omega^2-\Omega^2)^2+\omega^2\Gamma^2} \tag{27}$$

with the characteristic frequency $\Omega = v_l Q$ and a broadening Γ.

The Brillouin scattering thus gives a more or less well defined peak both in a constant-Q scan, which samples the scattering at different frequencies with a constant Q (provided Q is not too large), and in a constant-E scan, a scan at constant frequency $\omega = E/\hbar$ (E is the energy transfer of the scattering process), which samples the scattering for different values of the momentum transfer Q.

Neglecting the influence of Debye–Waller factors, the umklapp scattering from longitudinal and transverse sound waves in the long-wavelength limit is given by

$$S_U(Q,\omega) = S(Q)\frac{k_B T Q^2}{12\pi^2\rho}\left(\frac{1}{v_l^3}+\frac{2}{v_t^3}\right) \tag{28}$$

where ρ is the mass density and $S(Q)$ is the integrated scattering, which reflects the pair correlation functions of the atomic positions in the glass.

In the umklapp case, the constant-Q scan sampling the spectrum simply gives a constant intensity, though naturally each individual sound wave supplies a δ-function at its individual frequency. This constant intensity can be calculated from the density and the sound velocities, and is related to the constant in C_p/T^3 of equation (5). A constant-E scan in a fixed frequency window gives an intensity proportional to $Q^2 S(Q)$.

5.2. Scattering from other modes

If we again restrict ourselves to a classic approximation, the other modes coexisting with the sound waves might be either relaxational modes or vibrational modes. In the first case, the

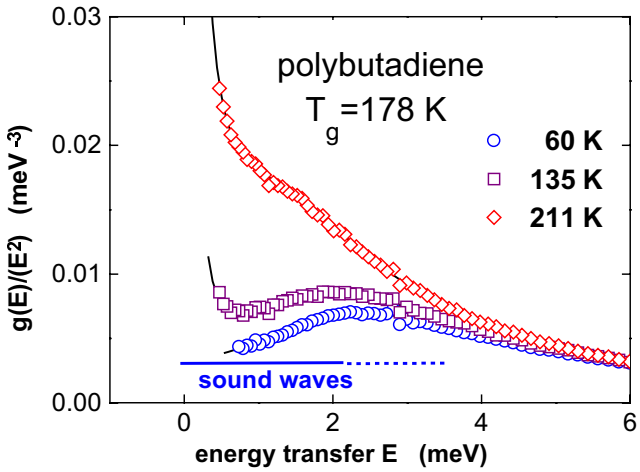

Figure 11. Neutron spectrum of amorphous polybutadiene divided by the Bose–Einstein factor at three different temperatures below and above the glass temperature $T_g = 178$ K.

spectrum is a Lorentzian $1/(1+\omega^2\tau^2)$ centred at the elastic line, where τ is the relaxation time of the mode. In the second, the spectrum is a δ-function at the frequency of the mode.

The existence of both kinds of additional mode is demonstrated in figure 11, a neutron measurement in polybutadiene at three different temperatures evaluated in terms of an effective vibrational density of states. At the lowest temperature of 60 K, one observes the boson peak at an energy transfer of 2.5 meV. Above that frequency, there is little change with temperature, indicating a vibrational density of states. But below the boson peak one finds the onset of relaxational motion already in the glass phase, and even more so above the glass transition. We conclude that there are both relaxational and vibrational modes coexisting with the sound waves.

One can learn about the eigenvector of these additional modes by doing constant-E scans, to look at the dynamic structure factor of the mode mixture in a given frequency window. Figure 12 shows such a measurement at the boson peak of vitreous silica (amorphous SiO_2). One finds an oscillating structure factor, but the oscillations are different from the $Q^2S(Q)$ expectation for the sound waves. Also, the intensity is a factor of eight too high compared to the Debye expectation. The experimental structure factor turned out to be well explained in terms of coupled librations of corner-connected SiO_4-tetrahedra (Buchenau *et al* 1988), a finding which has since been corroborated by simulation (Taraskin and Elliott 1997).

In order to evaluate such dynamic structure factor measurements in the inelastic scattering, one must be able to calculate the dynamic structure factor from the atomic displacements of a given mode. Let us assume a displacement $\vec{u}_j$ of atom j with scattering length b_j at the equilibrium position $\vec{R}_j$ in this mode. If one neglects the Debye–Waller factors, the dynamic structure factor $F(Q)$ in the one-phonon approximation reads

$$F(\vec{Q}) = \left| \sum_{j=1}^{N} \exp(\mathrm{i}\vec{Q}\vec{R}_j)\vec{Q}\vec{u}_j \right|^2 \tag{29}$$

where the sum goes over all N atoms of the glass. As long as one can reckon with the validity of the one-phonon approximation, the equation holds for both relaxation and vibration; if they have the same eigenvector, they have the same Q-dependence, though their spectrum is different.

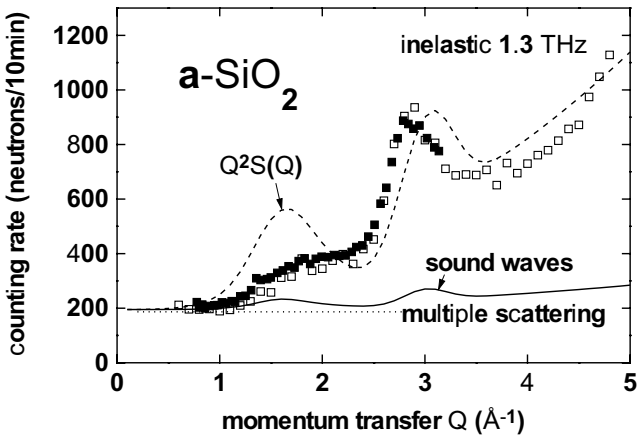

Figure 12. Dynamic structure factor at the boson peak of vitreous silica (Wischnewski *et al* 1998).

5.3. X-rays, neutrons and light

Light scattering measurements have a much better energy resolution than neutron and x-ray scattering, at least when one deals with the weak signals from relaxations and vibrations in glasses. For this case, the Raman technique can still resolve frequencies down to 8 GHz or 0.032 meV (Wiedersich *et al* 2000); the neutron technique can measure down to 0.5 meV and the inelastic x-ray scattering to 2 meV. As it chances, this latter limit happens to lie at the crossover from relaxation to vibration (see figure 11), so at present the inelastic x-ray scattering from glass excitations is restricted to measurements of vibrational excitations.

On the other hand, the Raman technique suffers from a poorly defined scattering cross section; at present, it is not possible in practice to calculate the Raman intensities for a given model of the motion. Also, varying the scattering angle practically does not change the Raman spectrum; one does not have the possibility to extract information from constant-E scans as in neutron and x-ray scattering. However, as we saw in figure 12 and as we will see from inelastic x-ray scattering examples, the constant-E scans provide very valuable information on the modes and their eigenvector, exactly the information which one wants to have.

The problem of the Raman information has been drastically demonstrated by a recent comparison of Raman and hyper-Raman scattering from vitreous silica (Hehlen *et al* 2000). Hyper-raman scattering is Raman scattering with simultaneous frequency doubling of the scattered light. It turned out that the hyper-Raman spectrum almost exactly reproduced the neutron spectrum, because the selection rule is such that one sees the coupled rotation of the corner-connected SiO_4-tetrahedra. The Raman spectrum has a completely different shape.

5.4. Brillouin and sub-Brillouin scattering

Though inelastic x-ray scattering is still a rather young technique, it is already clearly superior to neutron scattering at very small momentum transfer. Neutrons have a kinematic restriction: the relation $E_{max} = \hbar^2 Q^2/2m$ (m mass of the neutron) defines the maximum energy transfer one can attain at a given momentum transfer Q—and this requires a measurement at scattering angle zero. If one translates the relation into sound and neutron velocities, one finds that the neutron should have at least the longitudinal sound velocity to see the Brillouin scattering. Even then, a constant-Q scan will end at the phonon frequency; one can see the frequencies

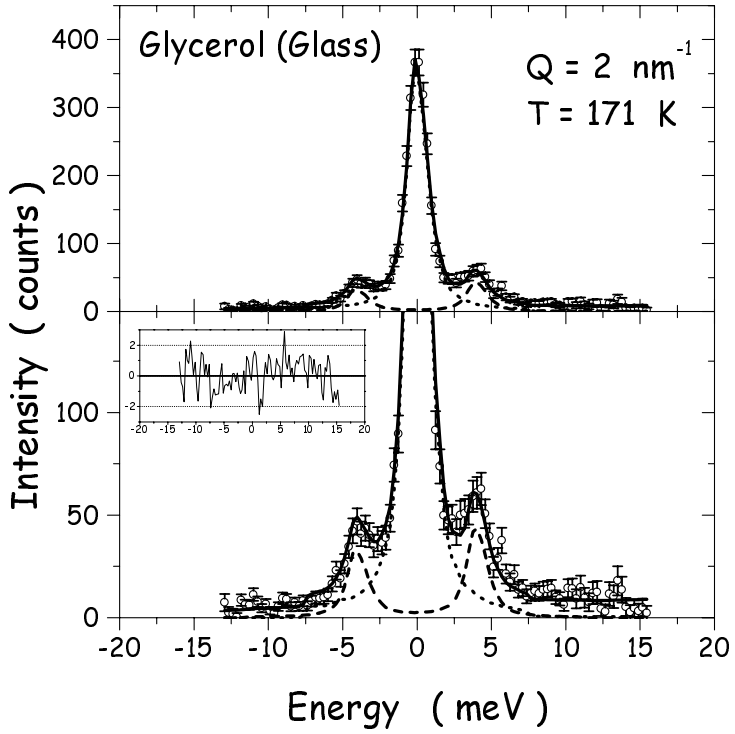

Figure 13. X-ray Brillouin scattering from glycerol just below the glass transition temperature: constant-Q scan (Masciovecchio *et al* 2000).

below the Brillouin line (and indeed one finds some sub-Brillouin scattering intensity there (Sokolov *et al* 1999, Russina *et al* 2000)), but one cannot measure to higher frequencies. X-rays do not have that problem, because the small energy transfer of a Brillouin scattering event is negligible compared to the energy of the x-ray quantum. On the other hand, x-rays have not yet attained the energy resolution of the neutron time-of-flight technique. Therefore the two techniques at present are complementary to each other (Sokolov *et al* 1999).

The high quality of recent inelastic x-ray Brillouin studies is demonstrated in figures 13 and 14 for glycerol at a temperature just below $T_g = 190$ K. Figure 13 shows a constant-Q scan, figure 14 two constant-E scans. Note that the scan at the lower energy of 4.7 meV shows again sub-Brillouin scattering intensity below the Brillouin line for 8 meV. This is consistent with the neutron results of sub-Brillouin scattering at much lower energies (Sokolov *et al* 1999, Russina *et al* 2000).

5.5. Umklapp scattering

For vitreous silica, we have seen in figure 12 that the inelastic scattering at the boson peak need not follow the $Q^2S(Q)$ behaviour predicted for the sound waves (Carpenter and Pelizzari 1975). In that particular case, one seems to have SiO_4 tetrahedron librations, which have a clearly distinct dynamic structure factor.

But naturally, each glass will have its own characteristic low-frequency vibrations, depending on which are the specific weak restoring forces of the system. In a polymer or in a large-molecule molecular glass like glycerol, the weak springs are the bond torsion motions,

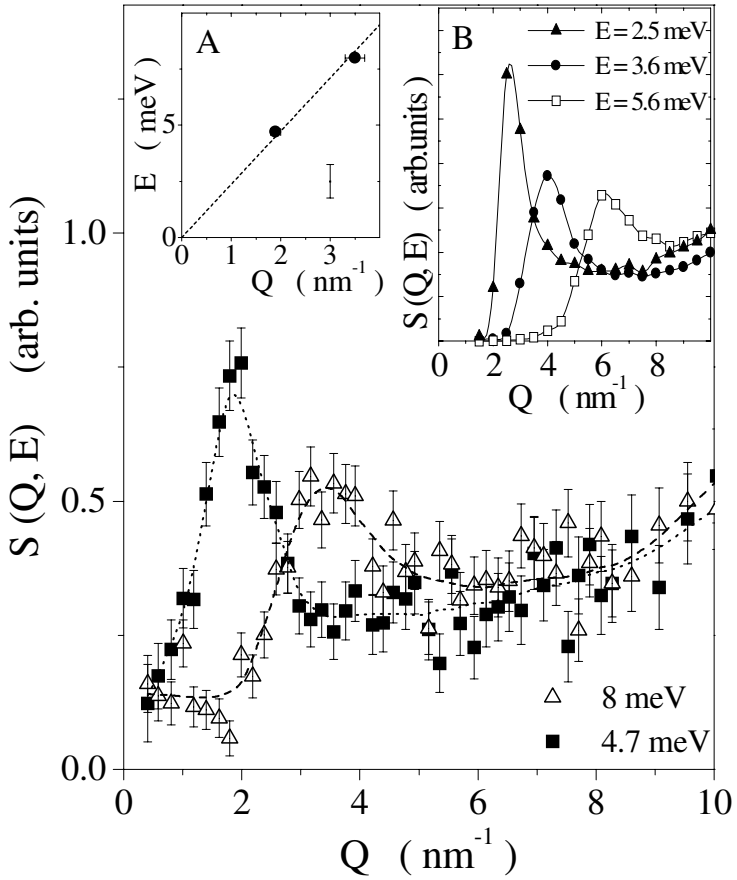

Figure 14. X-ray Brillouin scattering from glycerol just below the glass transition temperature: constant-E scans at 4.7 and 8 meV (Masciovecchio *et al* 2000). Inset A shows the extrapolation of the dispersion from low-frequency data (the broken line); inset B shows simulation results (Sampoli *et al* 1998).

together with the weak Van der Waals forces between different chains or molecules. In that case, the eigenvector of the soft motion is more difficult to visualize than in silica. In any case, the measurement of the dynamic structure factor in figure 15, again from the work of Masciovecchio *et al* (2000), shows that the first sharp diffraction peak in $S(Q)$ is reproduced in the dynamic structure factor of the inelastic scattering in glycerol, similar to neutron findings in polybutadiene (Sokolov *et al* 1999), but obviously different from the silica case.

The data show that the inelastic x-ray scattering technique begins to compete with neutron scattering also in the umklapp regime. This competition will turn out to be very valuable for the field of dynamics of glasses. The analysis of the mode eigenvectors in the region of the boson peak will be much easier, because again the two techniques are complementary. The x-rays tend to see mainly the motion of the heavier atoms, because the scattering length for x-rays is proportional to the number of electrons of a given atom. The scattering length for neutron scattering, in contrast, has nothing to do with the number of electrons around the nucleus, but is a purely nuclear property. To take one last time the example of silica, neutrons see mainly the oxygen, x-rays the silicon atoms. A correct model of the motion must be able to describe

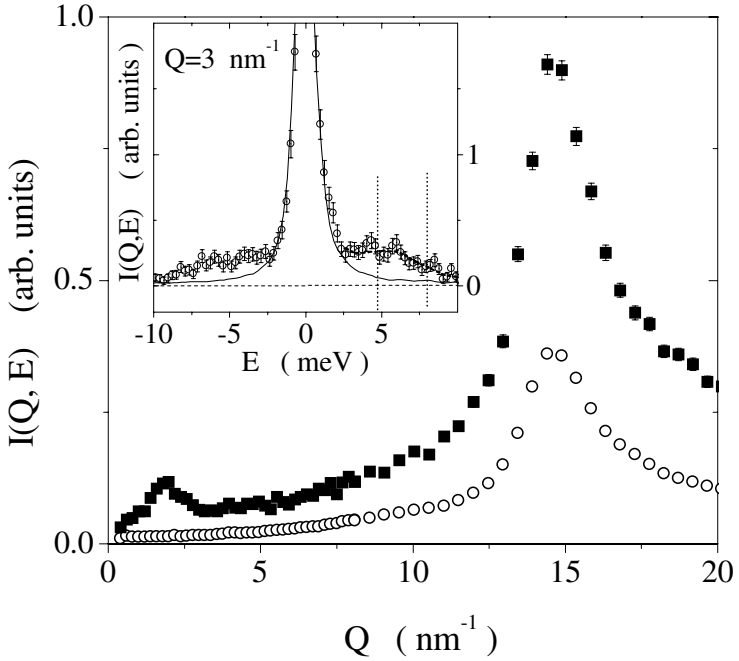

Figure 15. X-ray Brillouin scattering from glycerol just below the glass transition temperature: constant-E scan at 4.7 meV up to higher momentum transfer (Masciovecchio *et al* 2000). The inset shows the spectrum at small Q.

the dynamic structure factors of both techniques, which will differ from each other.

5.6. Summary and conclusions

We have taken a *tour de force* through the field of dynamics of glasses, beginning with the low-temperature anomalies of glasses and their description in terms of phenomenological models, the tunnelling model, the soft-potential model and the Gilroy–Phillips model. These three models are not in contradiction to each other. They are all based on the same idea, namely that local soft modes in glasses are influenced by the asymmetry of the surroundings and couple to the sound waves.

The Gilroy–Phillips model has the particular advantage of being very flexible, because it describes the classical Arrhenius relaxation in the glass phase in terms of a whole function, the barrier density function $f(V)$. As it turns out, the Gilroy–Phillips formalism can describe any relaxation, provided one allows for a temperature dependence of the barrier density function. Thus one can also describe the primary relaxation of the flow process at the glass transition, introducing two separate parts of the barrier density function with different temperature behaviour (Buchenau 2000). Note that the glass transition is not really explained. The Gilroy–Phillips formalism supplies only a reformulation of well known equations in terms of a barrier density function. It is a new way to look at the data, an encouragement to seek explanations in a new direction, complementary to attempts to understand the glass transition from the liquid side (Götze and Sjögren 1992), because it starts from a description of the relaxation in the glass phase. But it does not either explain the fast rise of the secondary relaxation above T_g, or supply a quantitative explanation of why the shear modulus breaks down completely when

it is halved by the secondary relaxation. It merely helps to quantify and to visualize these experimental facts.

In the last part of the paper, the present stage of the scattering studies of the low-frequency vibrational dynamics at the boson peak has been reviewed. There are beautiful new results from the inelastic x-ray scattering technique. Though inelastic x-ray scattering (at least for the purpose of studying low-frequency modes in glasses) is presently still limited to studies above 2 meV, it is preferable to neutrons if one wants to see a Brillouin line in a glass. The technique begins to be able to measure constant-E scans, also at higher momentum transfer Q. Thus one is able to combine Brillouin and umklapp scattering in a single measurement, as shown in figure 15. The results encourage the hope to develop a better understanding for the boson peak, which is still a puzzle.

References

Adam G and Gibbs J H 1965 *J. Chem. Phys.* **43** 139
Anderson P W, Halperin B I and Varma C M 1972 *Phil. Mag.* **25** 1
Angell C A 1995 *Science* **267** 1924
Angell C A and Rao K J 1972 *J. Chem. Phys.* **57** 470
Böhmer R, Ngai K L, Angell C A and Plazek D J 1993 *J. Chem. Phys.* **99** 4201
Buchenau U 2000 Mechanical relaxation in glasses and at the glass transition *Preprint* cond-mat/0008280
Buchenau U, Zhou H M, Nücker N, Gilroy K S and Phillips W A 1988 *Phys. Rev. Lett.* **60** 1318
Carpenter J M and Pelizzari C A 1975 *Phys. Rev.* B **12** 2391
Ediger M D, Angell C A and Nagel S R 1996 *J. Phys. Chem.* **100** 13 200
Ferry D J 1980 *Viscoelastic Properties of Polymers* 3rd edn (New York: Wiley)
Gilroy K S and Phillips W A 1981 *Phil. Mag.* B **43** 735
Götze W and Sjögren L 1992 *Rep. Prog. Phys.* **55** 241
Hehlen B, Courtens E, Vacher R, Yamanaka A, Kataoka M and Inoue K 2000 *Phys. Rev. Lett.* **84** 5355
Hunklinger S, Arnold W, Stein S, Nava R and Dransfeld K 1972 *Phys. Lett.* A **42** 253
Il'in M A, Karpov V G and Parshin D A 1987 *Zh. Eksp. Teor. Fiz.* **92** 291 (Engl. transl. *Sov. Phys.–JETP* **65** 165)
Jäckle J 1987 *Phil. Mag.* B **56** 113
Karpov V G, Klinger M I and Ignat'ev F N 1983 *Zh. Eksp. Teor. Fiz.* **84** 760 (Engl. transl. *Sov. Phys–JETP* **57** 439)
Koizumi S, Paciaroni A and Buchenau U unpublished
Kramers H A 1940 *Physica* **7** 284
Masciovecchio C, Mermet A, Ruocco G and Sette F 2000 *Phys. Rev. Lett.* **85** 1266
Mura T 1982 *Micromechanics of Defects in Solids* (The Hague: Martinus Nijhoff) p 63
Nittke A, Scherl M, Esquinazi P, Lorenz W, Li Yunyun and Pobell F 1995 *J. Low Temp. Phys.* **98** 517
Phillips W A 1972 *J. Low Temp. Phys.* **7** 351
——(ed) 1981 *Amorphous Solids: Low Temperature Properties* (Berlin: Springer)
Patterson G D 1977 *J. Polym. Sci.: Polym. Phys.* **15** 579
Plazek D J and O'Rourke V M 1971 *J. Polym. Sci.* A-2 **9** 209
Ramos M A and Buchenau U 1997 *Phys. Rev.* B **55** 5749
Russina M, Mezei F, Lechner R, Longeville S and Urban B 2000 *Phys. Rev. Lett.* **84** 3630
Sahnoune A, Massines F and Piché L 1996 *J. Polym. Sci.* B **34** 341
Sampoli M, Benassi P, Dell'Anna R, Mazzacurati V and Ruocco G 1998 *Phil. Mag.* B **77** 473
Schwarzl F R 1990 *Polymermechanik* (New York: Springer)
Sinnott K M 1962 *Soc. Plastics Eng. Trans.* **2** 65
Sokolov A P, Buchenau U, Richter D, Masciovecchio C, Sette F, Mermet A, Fioretto D, Ruocco G, Willner L and Frick B 1999 *Phys. Rev.* E **60** R2464
Sokolov A P, Novikov V N and Strube B 1997 *Europhys. Lett.* **38** 49
Surovtsev N V, Wiedersich J, Novikov V N, Rössler E and Sokolov A P 1998 *Phys. Rev.* B **58** 14 888
Taraskin S N and Elliott S R 1997 *Phys. Rev.* B **55** 117
Topp K A and Cahill D G 1996 *Z. Phys.* B **101** 235
Wiedersich J, Adichtchev S V and Rössler E 2000 *Phys. Rev. Lett.* **84** 2718
Wischnewski A, Buchenau U, Dianoux A J, Kamitakahara W A and Zarestky J L 1998 *Phys. Rev.* B **57** 2663
Yano O and Wada Y 1971 *J. Polym. Sci.* A-2 **9** 669
Zeller R C and Pohl R O 1971 *Phys. Rev.* B **4** 2029